2002GeoJI.151..221F

Geophys. J. Int. (2002) **151,** 221–234

The determination of source mechanisms of small earthquakes and revised models of local crustal structure by moment tensor inversion

R. W. Ferdinand[1,2] and R. Arvidsson[2]

[1] *Physics Department, University of Dar es Salaam,* PO Box 35063 *Dar es Salaam, Tanzania*
[2] *Department of Earth Sciences, Uppsala University, Villavagen* 16, *Uppsala* S-752 36, *Sweden. E-mail: rf@geofys.uu.se*

Accepted 2002 May 3. Received 2002 April 22; in original form 2001 February 2

SUMMARY

We describe a procedure for retrieving the source mechanism of small earthquakes and a revised model of crustal structure in heterogeneous media based on interactive inversion of high frequency seismograms and demonstrate its application to three local earthquakes. The earthquakes are located along the Rukwa rift, south-western Tanzania, and were recorded by a local network in the rift. Due to strong lateral crustal heterogeneity in the area, the procedure involves a single-station interactive inversion for moment tensor solution and modelling of the crustal structure along the propagation path between the source and the station. Based on this source solution and the *a priori* crustal structure, synthetic seismograms are generated and compared with observed displacement seismograms at other stations where the event has been recorded. Deviations between the calculated and observed seismograms are indicated by time shifts and amplitude mismatches on prominent phases; these are employed to correct the phase arrivals used to invert for the partial multistation source solution. The moment tensor inversion of high frequency seismogram data in this study is based on a point source approach. The process includes generation of synthetic seismograms using the frequency-wavenumber integration technique for an elastic, horizontally-layered, medium. Moment tensor inversion is carried out by minimizing the L2 norm of the difference between synthetic and observed displacement data under a deviatoric condition. Results for the three small earthquakes show good agreement between single station and multistation source solutions. The inversions for these events indicate dominantly dip-slip mechanisms with seismic moment magnitudes in the range $2.0 \leq M_w \leq 3.3$.

Key words: moment tensor inversion, source mechanism.

1 INTRODUCTION

Earthquake source mechanisms are of prime importance in the monitoring of local, regional and global seismicity, because they reflect the stress pattern acting in the area under study and may help to map its tectonic structure. On a global scale, sources of information are large and moderate earthquakes that occur in active tectonic regions and are recorded by seismic stations worldwide. Techniques for analysing these data are well established, that is, from first motion polarity readings analysis to waveform modelling of surface and long period body waves (Langston & Helmberger 1975; Given *et al.* 1982; Dziewonski & Woodhouse 1983; Nabelek 1984; Sipkin 1986). Advantages on such teleseismic studies included the availability of recording stations that cover the source region and the simplicity of waveforms and structures involved. At regional and local scale however, the scope for such studies is limited due to the limited number of recording stations and their spatial distribution. This leads to a problem in obtaining reliable source information from regions where the majority of earthquakes are small. As a result of the wide deployment of highly sensitive digital seismic instruments, high quality waveform data from small earthquakes can now be obtained from regional or local networks. However, data from such networks are not simple to analyse. Reasons for this include the influence of heterogeneous structure between the source and the recording station and the dominance of high frequencies in the signal.

In general, the observed seismograms contain information about the source, the path and the recording instrument. The practical problem is to isolate information about the source by correcting for the path and instrumental effects. The effect of the instrument is easily removed because the instrumental response is known, on the other hand isolating the path effect relies on the linear relationship between the observed ground displacement and seismic moment tensor density (Gilbert 1970; Stump & Johnson 1977; Aki & Richards 1980; Jost & Herrmann 1989). In practice, however, complete isolation of the path effect has proved difficult because a simple point source approach and flat layered structure model are not always good approximations, especially for high frequency data

© 2002 RAS

© Royal Astronomical Society • Provided by the NASA Astrophysics Data System

2002GeoJI.151..221F

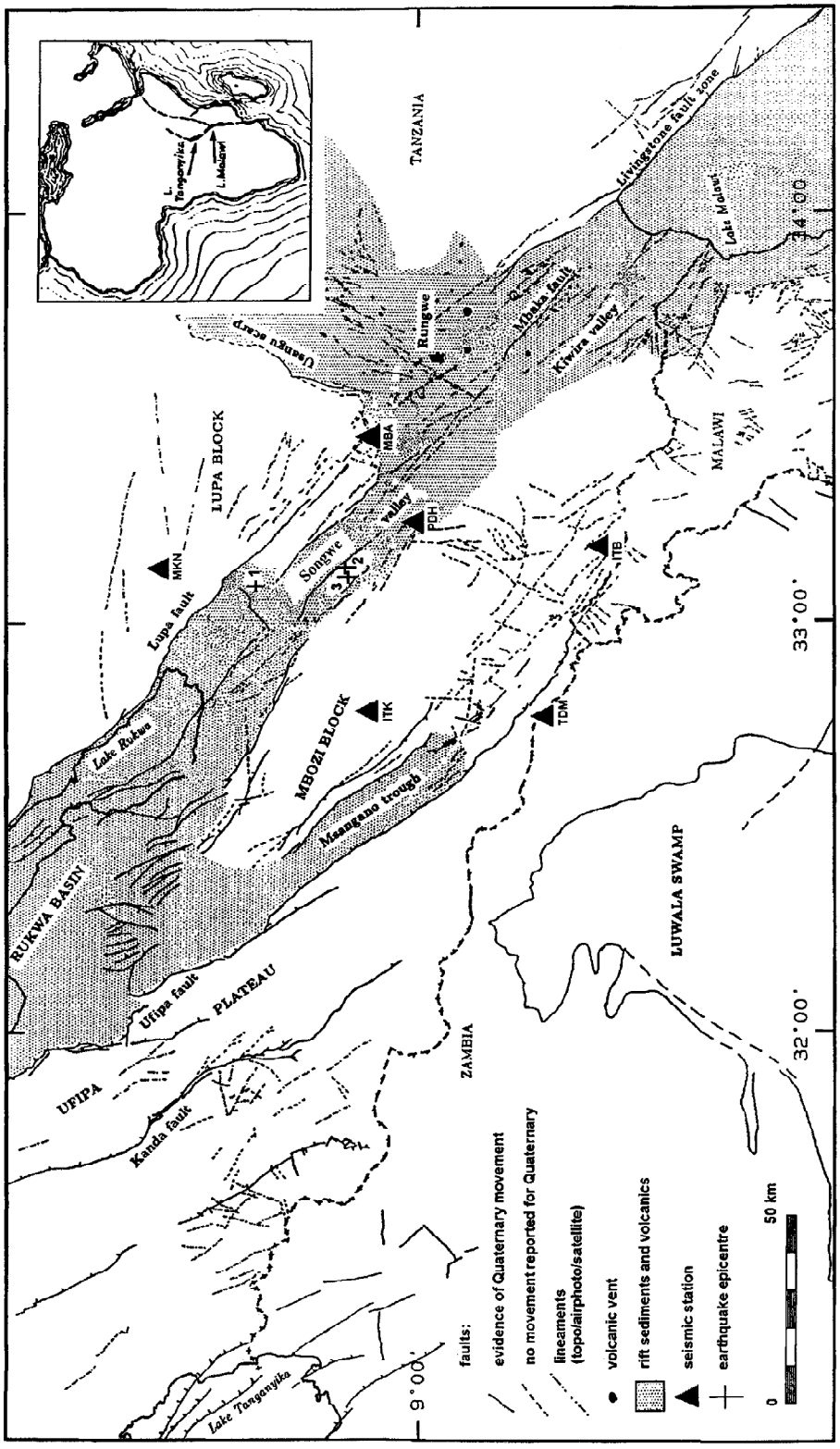


Figure 1. Map of the South Rukwa–North Malawi area showing the following features: geological information and the location of the Mbeya local network following the work of Camelbeeck & Iranga (1996) and epicentres of three selected earthquakes along the Rukwa rift. The numbers are in reference to Table 2.

© Royal Astronomical Society • Provided by the NASA Astrophysics Data System

2002GeoJI.151..221F

Table 1. Locations of seismic stations of the Mbeya network.

Station	Abr.	Latitude S	Longitude E	Elevation (m)
Panda Hill	PDH	8°58.99′	33°14.50′	1340
Makongolosi (2)	MKN	8°24.80′	33°10.13′	1500
Mbeya (1)	MBA	8°52.44′	33°27.17′	1780
Itaka	ITK	8°52.37′	32°46.98′	1590
Itumba	ITB	9°25.72′	33°11.15′	1270
Tunduma	TDM	9°17.77′	32°46.27′	1590

(1) Operated from June 15, 1992 to March 15, 1993.
(2) Operated since March 16, 1993.

(Lay & Wallace 1995). As propagation effects can never be fully excluded, they give rise to mislocation of the hypocenter and spurious source complexities.

To address the above problem, various approaches have been developed based on moment tensor inversion in the time or frequency domain (Saikia & Herrmann 1985; Kim 1987; Fan & Wallace 1991; Koch 1991a; Arvidsson & Kulhanek 1994; Arvidsson 1996; Zhu & Helmberger 1996; Shomali & Slunga 2000; Singh *et al.* 2000). These methods differ mainly in the nature of the problem that sets the *a priori* constraints. In trying to minimize the influence of the crustal structure, which is normally associated with a time-shift of the various phases in a seismogram, different segments of seismogram, that is, P, S, P_{nl}, Rayleigh , Love etc., have been modelled separately (Zhao & Helmberger 1994; Nabelek & Xia 1995). The advantage of this approach is that each phase is aligned using its onset time instead of the origin time. The various phase shifts obtained can then be used to correct for the crustal structure. Assuming that direct P and S phases from shallow events at close epicentral distances are less affected by crustal structure, Schurr & Nabelek (1999) managed to obtain mechanisms for the aftershock sequence of the 1993 Scotts Mills event. Apart from modelling different segments of seismograms mentioned above, simultaneous inversion of both the source and the structure has been applied on full trace high frequency data in a less heterogeneous structure (Sileny *et al.* 1992; Sileny & Pšenčik 1995). In their approach, both the hypocenter and the structure are allowed to vary in a limited sense in order to obtain the best fit between the observed and synthetic data. In areas of strong lateral heterogeneity the approach has been modified by the use of different source–receiver propagation structures that produce the best fit (Mao *et al.* 1994; Sileny *et al.* 1996; Singh *et al.* 2000).

In this study, we use an interactive inversion approach to demonstrate the retrieval of the source parameters of three small earthquakes along the Rukwa rift (Fig. 1) and developed a modified model of structure along the propagation path. The structure of Nyanza craton (KRISP 1991) is used as an initial model to generate synthetic seismograms for inversion. Due to significant variation of structure throughout the Mbeya local network (Camelbeeck & Iranga 1996), a single station approach is used. Using trial and error, the initial structure along the propagation path is modified to obtain the best fit between observed and synthetic data. The final single station solution is then used to generate synthetics for forward modelling of the seismograms at other stations where the event was recorded. Deviations between synthetics and observed data allowed us to deduce structural differences along the various propagation paths. Finally, a partial multistation solution was produced by inverting only those phases which showed a small deviation.

2 DATA

The data set used in this study is part of the data used by Camelbeeck & Iranga (1996) in their work on identifying active faults along the Rukwa trough. These data were recorded by stations of the Mbeya network during the period June 1992 to December 1994. The Mbeya network, the geology and tectonic setup of the Rukwa rift is described in Camelbeeck & Iranga (1996). Table 1 lists the coordinates of the Mbeya network stations. From the data set, three events were selected. Table 2 gives location parameters and magnitudes of these events as given by Camelbeeck & Iranga (1996) and Fig. 1 shows epicenter and station distributions along the Rukwa rift.

Preliminary locations of recorded events were determined using a homogeneous, one layer crustal model overlaying a half-space (Camelbeeck & Iranga 1996). Due to the high frequency nature of the observed seismograms (Fig. 2), a multilayered medium might be expected to give a better representation (Saikia & Herrmann 1985; Fan & Wallace 1991). Several multilayered crustal structures have been determined along the eastern and western branch of the East African rift (Table 3), but none of them is centred under the study area. Due to geological similarities in structure between the study area and the Nyanza craton (KRISP 1991), that is, they lie between the cratonic and proterozoic regions, the multilayered structure around the Nyanza craton has been adopted in previous work (Camelbeeck & Iranga 1996; Zhao *et al.* 1997). In the present study, this structure was used as an initial model. Based on this model, hypocenter solutions of the events selected were obtained using arrival times of P and S phases in HYPOINVERSE (Klein 1984). The arrival times at each station were picked from three-component seismograms using the SEISAN program (Havskov 1997).

3 METHODOLOGY

Our approach is limited to the far field approximation of a point source. Following Aki & Richards (1980), if a point source equivalent of the extended source is assumed, the nth component of the ground displacement U_n at an arbitrary position r at time t can be expressed as

$$U_n(t) = G_{nk,j}(t) \otimes \boldsymbol{M}_{kj}(t) \tag{1}$$

where $G_{nk,j}$ is the jth spatial derivative of the far field elastodynamic Green's function $G_{nk}(r, x, t)$ for the Earth between the source and

Table 2. Events used in this study.

Event number	Date	Origin time	Latitude S	Longitude E	Depth (km)	Mag. (M_L)	No. station	rms
1	920625	09:14:01.7	8°33.65	33°05.57	21.6	2.8	5	0.17
2	920704	13:41:55.2	8°47.40	33°12.84	18.6	2.7	5	0.12
3	920909	08:59:09.5	8°46.96	33°12.27	20.2	2.0	4	0.12

rms: miss-determination of origin time in seconds.

© Royal Astronomical Society • Provided by the NASA Astrophysics Data System

2002GeoJI.151..221F

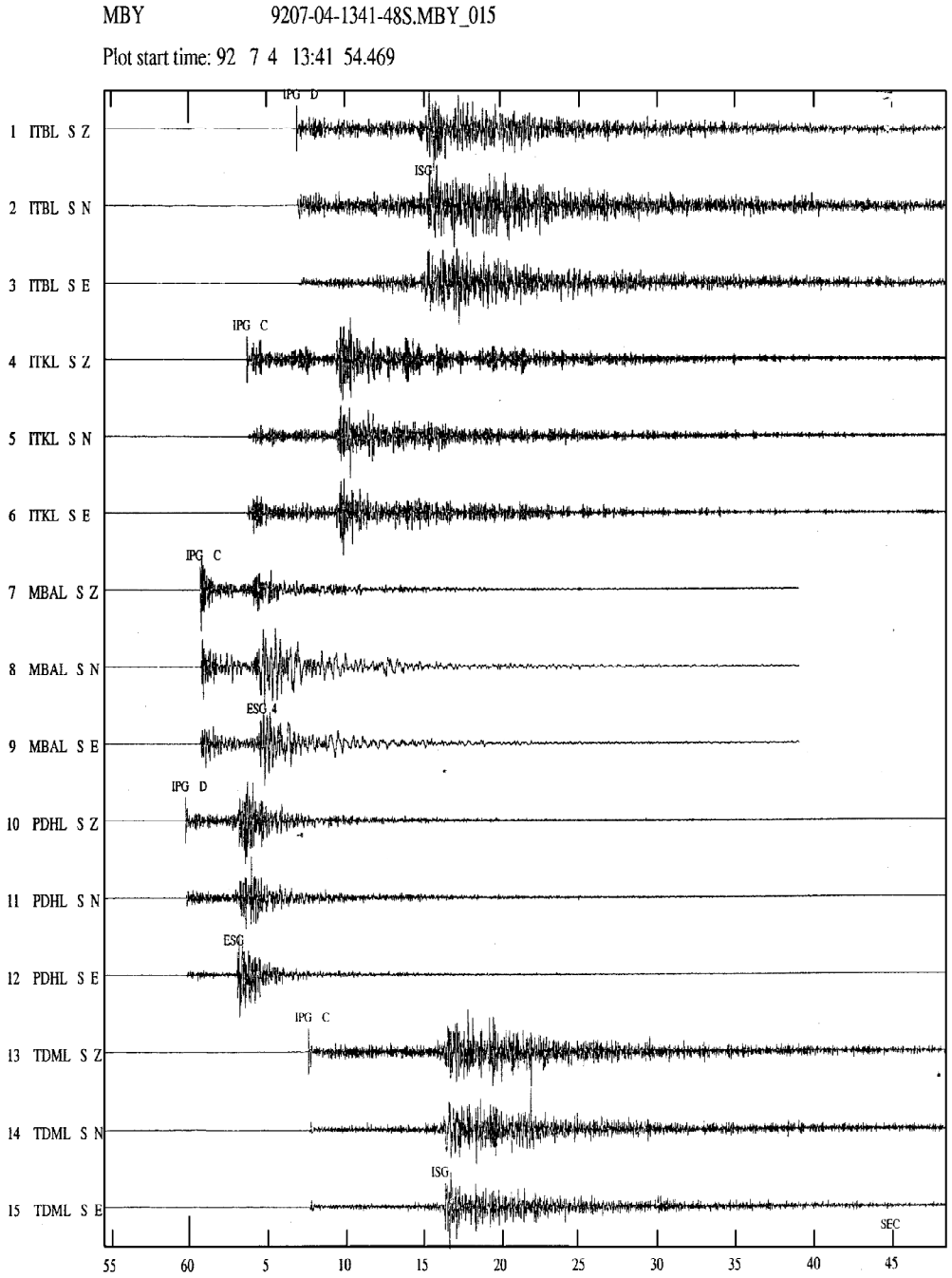


Figure 2. Typical observed short period, three component seismograms from a earthquake (event 2 in Table 2) located along the Rukwa rift and recorded by five stations of the Mbeya network.

receiver, $\boldsymbol{M}_{kj}$ is the moment tensor at the hypocenter point x and $\otimes$ denotes temporal convolution. Assuming that all components of $\boldsymbol{M}_{kj}$ in (1) have the same time dependence, say $s(t)$, (1) becomes

$$U_n(t) = \boldsymbol{M}_{kj}(G_{nk,j}(t) \otimes s(t)) \tag{2}$$

where $\boldsymbol{M}_{kj}$ is now a set of constants and $s(t)$ is the source time function. The intention is to use observed ground displacements U_n to infer properties of the source as characterised by $\boldsymbol{M}_{kj}$.

The Green's functions were prepared using the frequency-wavenumber (F-K) integration method (Bouchon 1981). Fortran code written by Herrmann (1996) was used to compute the complex spectra of eight Green's function components associated with slip on the three fundamental faults caused by an arbitrary shear dislocation point source in a plane layered elastic medium. The Fourier transform of the displacement at the free surface at the distance r from the origin, due to an arbitrary oriented double couple without moment, in cylindrical coordinate system, is

© Royal Astronomical Society • Provided by the NASA Astrophysics Data System

2002GeoJI.151..221F

Table 3. Crustal structure models from different studies along the eastern branch (EB) and western branch (WB) of the East African rift system.

Thickness (km)	Vp (km s^{-1})	Vs (km s^{-1})	Region	Author
26	5.8 ± 0.2		Western flank of EB	1
18	6.5 ± 0.3			
	8.0 ± 0.1			
14	5.9		Nyanza craton	2
13	68			
10	6.8			
	8.0			
12	5.9		Eastern flank of EB	2
18	6.5			
6	6.8			
	8.0–8.1			
3	4.9		Axial part of EB	2
6	6.1			
16	6.6			
6	6.8			
	7.5			
14	5.8	3.61	Northern part of WB	3
21	6.46	3.86		
	7.97	4.7		
42	6.2 ± 0.2		Southern part of WB	4
	8			
41.3 ± 7.5	6.32 ± 0.256	3.61 ± 0.016	WB	5
	8.11 ± 0.046	4.67 ± 0.053		

(1) Maguire & Long (1976); (2) KRISP working party (1991); (3) Nolet & Muller (1982); (4) Camelbeeck & Iranga (1996); (5) Ferdinand & Camelbeeck (2000).

$$
\begin{aligned}
U_z &= 0.5(Z_{SS}\cos 2\phi' - Z_{DD})M_{xx} \\
&\quad - 0.5(Z_{SS}\cos 2\phi' + Z_{DD})M_{yy} + Z_{SS}\sin 2\phi' M_{xy} \\
&\quad + Z_{DS}\cos\phi' M_{xz} + Z_{DS}\sin\phi' M_{yz} \\
U_r &= 0.5(R_{SS}\cos 2\phi' - R_{DD})M_{xx} \\
&\quad - 0.5(R_{SS}\cos 2\phi' - R_{DD})M_{yy} + R_{SS}\sin 2\phi' M_{xy} \\
&\quad + R_{DS}\cos\phi' M_{xz} + R_{DS}\sin\phi' M_{yz} \\
U_t &= 0.5T_{SS}\sin 2\phi' M_{xx} - 0.5T_{SS}\sin 2\phi' M_{yy} \\
&\quad - T_{SS}\cos 2\phi' M_{xy} + T_{DS}\sin\phi' M_{xz} - T_{DS}\cos\phi' M_{yz}
\end{aligned}
\tag{3}
$$

where U_z, U_r and U_t are vertical, radial and tangential displacements, respectively (Herrmann & Wang 1985; Jost & Herrmann 1989). Functions Z_{SS}, R_{SS}, T_{SS}; Z_{DS}, R_{DS}, T_{DS} and Z_{DD}, R_{DD} are the components of the Green's functions required to calculate the wavefield due to an arbitrary point dislocation source buried in a layered medium for the three fundamental orientations, that is, vertical strike-slip, vertical dip slip and 45° dip slip respectively. These Green's functions have been multiplied by a normalized Fourier transform of a source time function approximated by a triangular pulse. The M_{ij} are components of the moment tensor and ϕ' is the azimuth angle between source and station. The Green's functions were calculated using the hypocenter solution and the crustal structure model. The resulting spectra of the Green's function components were then transformed into the time domain by inverse Fourier transformation.

Prior to inversion, the analysis procedure included removal of the instrumental response, rotation of the horizontal components, windowing, bandpass filtering and alignment of the observed data to the

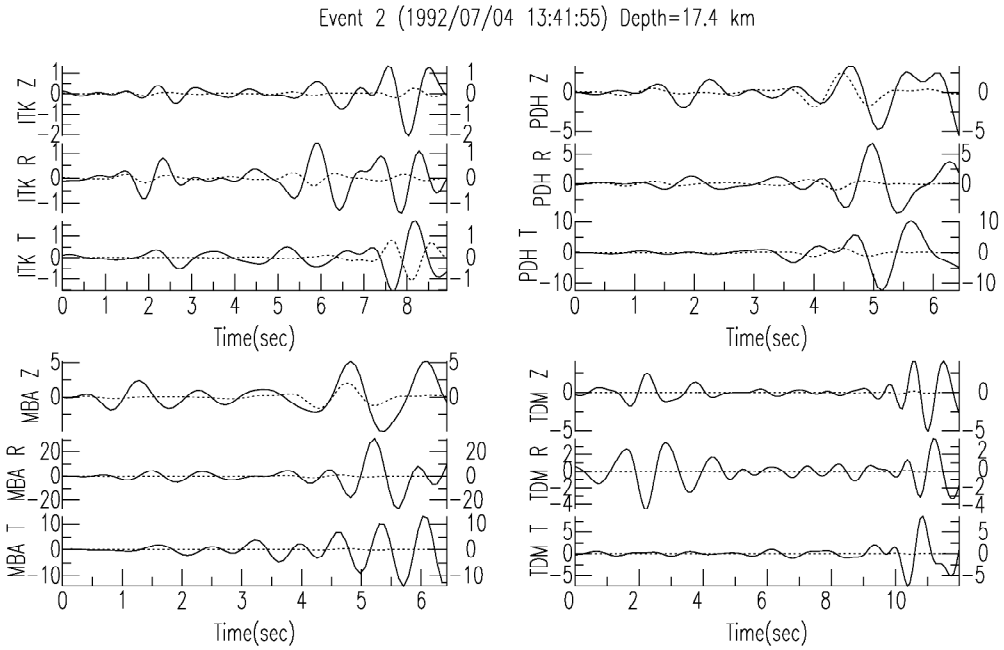


Figure 3. Moment tensor inversion results for event 2 (Table 2) based on synthetics generated using the Nyanza craton crustal structure model (K-model) in Table 3. The solid lines are the observed data, and the dashed lines are synthetics. Time is referred to the beginning of the window and the vertical scale is in microns. The station identifiers used, that is, ITB, ITK, etc. are as indicated in Table 1. Z, R and T stand for vertical, radial and transverse components respectively.

© Royal Astronomical Society • Provided by the NASA Astrophysics Data System

2002GeoJI.151..221F

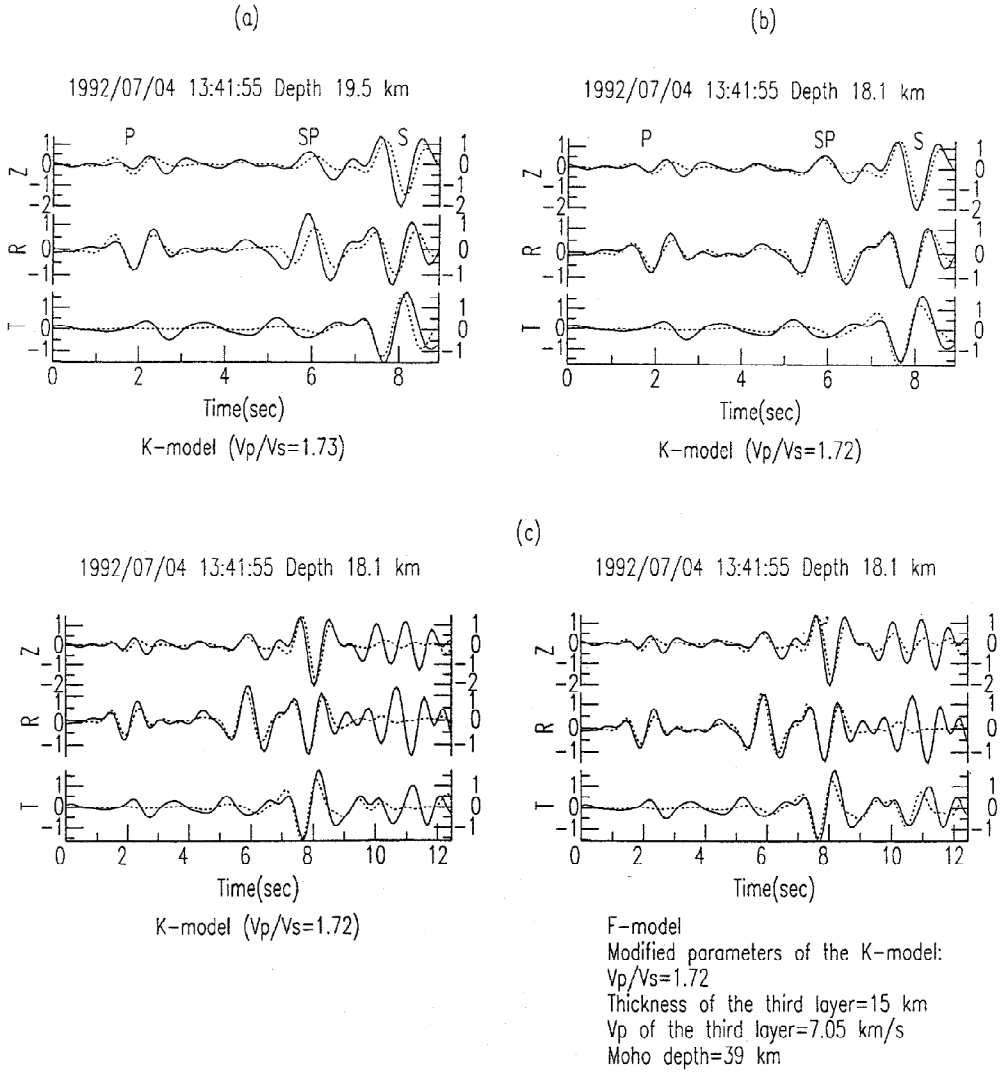


Figure 4. Single station moment tensor inversion results of event 2 (Table 2) based on synthetics generated using the K-model in (a) and the K-model with $Vp/Vs = 1.72$ in (b). Comparison between single station moment tensor inversion results of 12.5 s window for event 2 based on synthetics generated by using the K-model with $Vp/Vs = 1.72$ and F-model in (c). The solid lines are the observed data, and the dashed lines are synthetics. The window is 9 s long and the time is referred to the beginning of the window. The vertical scale is in microns and Z, R and T are as explained in Fig. 3.

synthetics. The observed data were transformed in the frequency domain, where the effect of the instrumental response was removed in order to obtain ground motion as displacement. The observed displacement data were then transformed back into the time domain, where the horizontal components were rotated from east-west and north-south to transverse and radial using the backazimuth angle calculated from the hypocenter solution. Lack of *P*-wave arrivals on the tangential displacement component was taken as indicating that the source-receiver azimuth had been properly determined. Both the observed and synthetic data were windowed using a cosine taper. Although most of the information necessary for determining the earthquake moment tensor is contained in direct *P*, *SH* and *SV* pulses, recorded respectively on the Z (vertical), T (transverse) and R (radial) components, we preferred to take the analysis window from one second before the beginning of *P* to the beginning of the multiple *S* phase. This was important because we also aimed at improving the adopted Nyanza craton structure by fitting phases other than direct *P* and *S*. To obtain simple and distinct phase pulses, a bandpass filter was applied to both observed and synthetic data. The high-pass cut-off was determined by the signal power at low frequencies, whereas the ability to simulate the observed data sets the low-pass cut-off. After several trials a band between 0.6 and 1.5 Hz was adopted and applied to all selected events. Finally, observed and synthetic data within each window were aligned with respect to the origin time.

By convolving the Green's functions with a normalized source time function eq. (2) can be written as

$$\mathbf{U} = \mathbf{G}'M \tag{4}$$

where $\mathbf{U}$ is a $(N \times 1)$ vector, composed of ground displacements in all components, N is the total number of data in all traces used, $\mathbf{M}$ is a (5×1) vector consisting of five components of the moment tensor and $\mathbf{G}'$ is a $(N \times 5)$ matrix composed of Green's function components convolved with the normalized source time function. The number of independent components of the moment tensor in (4) is

© Royal Astronomical Society • Provided by the NASA Astrophysics Data System

2002GeoJI.151..221F

Table 4. Moment tensor inversion results and fault plane solutions of event 2 obtained using Nyanza craton model.

	K-model ($Vp/Vs = 1.73$)	K-model ($Vp/Vs = 1.72$)
M_{xx} ($\times 10^{12}$ N m)	1.360 ± 0.180	1.730 ± 0.093
M_{yy} ($\times 10^{12}$ N m)	-0.436 ± 0.127	-0.468 ± 0.041
M_{xy} ($\times 10^{12}$ N m)	0.400 ± 0.408	0.779 ± 0.083
M_{xz} ($\times 10^{12}$ N m)	-3.260 ± 1.830	-6.890 ± 0.499
M_{yz} ($\times 10^{12}$ N m)	0.384 ± 0.259	0.995 ± 0.080
M_0 ($\times 10^{12}$ N m)	3.000	6.830
$E_{\rm rms}$ (μm)	0.35	0.25
Strike (deg)	310, 83	319, 82
Dip (deg)	13, 81	10, 84
Slip (deg)	$-44, -100$	$-34, -98$
Depth (km)	19.5	18.1
CLVD per cent	18	6

reduced to five by imposing a deviatoric condition. The observed data are inverted using a generalized inverse technique employing components of **M** that minimize the difference between observed and synthetic seismograms in a least-squares sense (Stump & Johnson 1977). In order to obtain the best fit, several inversions were performed for a suite of focal depths. The summed root-mean squared (rms) error measures the goodness of fit and can be written as:

$$E_{\rm rms} = \sum_{i=1}^{l} \sqrt{\frac{1}{m} \sum_{j=1}^{m} (U_j - C_j)^2} \qquad (5)$$

where U and C are observed and predicted ground displacements respectively, l is the number of components and m is the total number of samples within the inversion window for each component. The source depth corresponding to the minimum rms value provides the means for determining the focal depth and source parameters. Because the value of $E_{\rm rms}$ is related to the size of the event, the normalized variance was used where fits from different events needed to be compared (Zhao & Helmberger 1994). The reliability of the moment tensor solution depends on the error estimate for each component (Stump & Johnson 1977).

Table 6. Moment tensor inversion results and fault plane solutions of event 2 obtained by using the K-model with $Vp/Vs = 1.72$ and F-model for a 12.5 s. 3-component time section. The modified parameters in F-model are listed below the table.

	K-model ($Vp/Vs = 1.72$)	Modified Kenyan model (F-model)
M_{xx} ($\times 10^{12}$ N m)	1.440 ± 0.145	1.550 ± 0.126
M_{yy} ($\times 10^{12}$ N m)	-0.407 ± 0.063	-0.383 ± 0.053
M_{xy} ($\times 10^{12}$ N m)	0.653 ± 0.117	0.498 ± 0.081
M_{xz} ($\times 10^{12}$ N m)	-5.870 ± 0.699	-5.190 ± 0.484
M_{yz} ($\times 10^{12}$ N m)	0.794 ± 0.113	0.713 ± 0.080
M_0 ($\times 10^{12}$ N m)	5.77	5.090
$E_{\rm rms}$ (μm)	0.395	0.367
Strike (deg)	319, 83	311, 83
Dip (deg)	10, 85	10, 83
Slip (deg)	$-34, -98$	$-42, -98$
Depth (km)	18.1	18.1
CLVD per cent	8	8
Modified parameters:		
Vp/Vs—1.72		
Thickness of the third layer—15 km		
Vp of the third layer—7.05 km s^{-1}		
Moho depth—39 km		

The best deviatoric moment tensor solution was decomposed into a double couple (DC) with a compensated linear vector dipole (CLVD) as the remaining non-double couple part (Geller 1976). In this work, the percentage contribution of the CLVD and $E_{\rm rms}$ together is used as a measure of the error due to unmodelled effects in the moment tensor inversion. These effects are ascribed to noise

Table 5. Hypocenter solutions of the selected events obtained using the F-model.

Event 1							
Date	Origin time	Latitude S	Longitude E	Depth (km)	rms	erlt (km)	erln (km)
920625	09:14:02.5	8°36.84′	33°05.70′	17.4	0.05	8.6	5.7
Station	Distance (km)	Azimuth	Take-off angle				
PDH	44	158	103				
ITK	45	230	103				
TDM	83	205	94				
ITB	91	174	93				
Event 2							
Date	Origin time	Latitude S	Longitude E	Depth (km)	rms	erlt (km)	erln (km)
920704	13:41:55.2	8°48.23′	33°12.09′	18.1	0.08	8.1	6.5
Station	Distance (km)	Azimuth	Take-off angle				
PDH	20	171	129				
MBA	27	106	120				
ITK	48	261	103				
TDM	73	222	96				
ITB	69	183	96				
Event 3							
Date	Origin time	Latitude S	Longitude E	Depth (km)	rms	erlt (km)	erln (km)
920909	08:59:09.8	8°48.27′	33°11.50′	15.5	0.08	5.7	3.5
Station	Distance (km)	Azimuth	Take-off angle				
MBA	30	105	110				
ITK	46	260	103				
TDM	71	220	92				
ITB	69	181	92				

© Royal Astronomical Society • Provided by the NASA Astrophysics Data System

2002GeoJI.151..221F

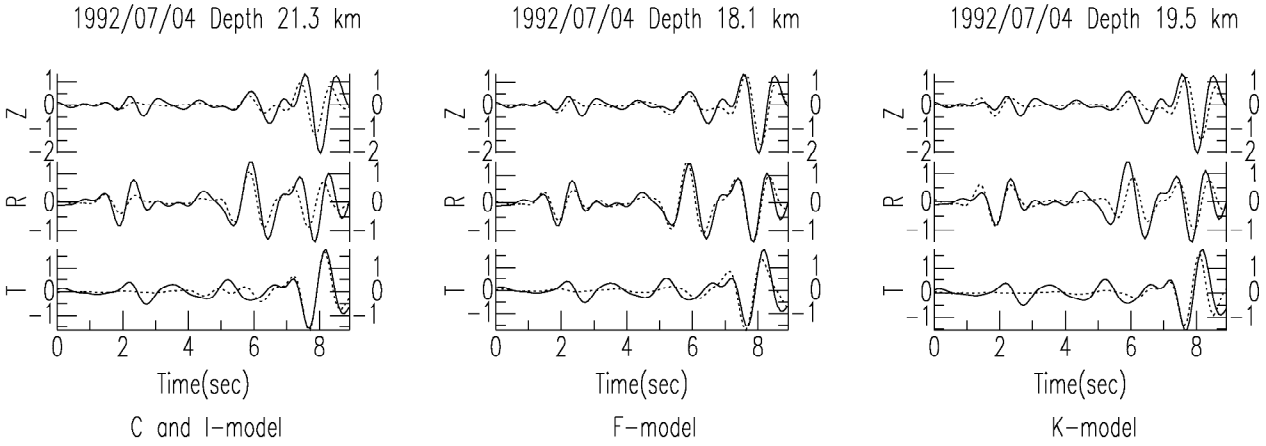


Figure 5. Comparison of single station moment tensor inversion results of a 9-s window for event 2 based on synthetics generated by using the C and I-model in Table 3, F-model and K-model.

Table 7. Comparison of moment tensor inversion results and fault plane solutions of event 2 obtained using three different crustal structure models.

	(K-model)	(F-model)	(C & I-model)
M_{xx} ($\times 10^{12}$ N m)	1.360 ± 0.180	1.690 ± 0.087	-1.320 ± 0.264
M_{yy} ($\times 10^{12}$ N m)	-0.436 ± 0.127	-0.469 ± 0.040	2.280 ± 0.221
M_{xy} ($\times 10^{12}$ N m)	0.400 ± 0.408	0.795 ± 0.078	-6.020 ± 0.535
M_{xz} ($\times 10^{12}$ N m)	-3.260 ± 1.830	-6.920 ± 0.472	14.80 ± 1.340
M_{yz} ($\times 10^{12}$ N m)	0.384 ± 0.259	0.997 ± 0.076	-2.740 ± 0.265
M_0 ($\times 10^{12}$ N m)	3.000	6.860	16.100
M_w	2.8	3.3	3.8
$E_{\rm rms}$ (μm)	0.355	0.24	0.356
Strike (deg)	310, 83	320, 82	79, 173
Dip (deg)	13, 81	10, 85	88, 23
Slip (deg)	$-44, -100$	$-33, -98$	$-67, -175$
Depth (km)	19.5	18.1	21.3
CLVD per cent	18	6	2

and because the use of a simple flat layered model used to generate the Green's functions and simple source time function may not be the best representation of the structure and source, respectively. The double couple part, on the other hand, was used to calculate the double couple seismic moment, M_0, and the pressure and tension axes. The value of M_0 was obtained from the eigenvalues while the pressure and tension axes were obtained from the eigenvectors (Jost & Herrmann 1989). The fault orientation, that is, strike, dip and rake was calculated from the pressure and tension axes. The value of M_0 was then used to calculate an estimate of the moment magnitude, M_w (Hanks & Kanamori 1979).

4 RESULTS AND DISCUSSION

The method outlined in the preceding section was applied to three events located along the Rukwa rift. In this section, the second event in Table 2 (1992 07 04) is used to explain the waveform modelling procedure and method of revision of the crustal structure model. From the hypocenter solution obtained using the Nyanza craton structure model in Table 3 (subsequently referred to as the K-model), synthetic seismograms were produced and fitted to observed data recorded at four stations of the Mbeya network. Fig. 3 shows the synthetic and observed seismograms. From the figure it is seen that the source-receiver azimuth is well determined at all stations. A clear phase shift and amplitude mismatch between synthetic and observed data can be noticed at all stations and it is especially well pronounced at ITK station. This might be due to heterogeneity within the shallow local structure (Camelbeeck & Iranga 1996; Ferdinand 1998). At such short epicentral distances, the receiver crustal structure plays an important role in shaping the waveform, especially at high frequencies (Helmberger & Johnson 1977). To overcome these problems we decided to use a single station approach.

4.1 Single station solution and improvement of the propagation path structure

The information from a single station with three-component recordings is normally considered insufficient to retrieve the full moment tensor components as it is believed to come from mainly three direct phases, that is, P, S_V and S_H (Sileny *et al.* 1996). However, full traces from three-component single stations at certain epicentral distances and azimuths show clear phases in addition to the direct phases mentioned above, for instance, free surface converted phases or Moho reflected and converted phases, such as *SP*, *PmP*, *SmS* etc. Since these phases leave the focal sphere at different angles they carry additional information about the source. Since these phases are more related to the crustal structure, they are more difficult to fit as the detailed structure is not necessarily well known. Successful fitting of a suite of 3-component seismograms from a single station therefore requires simultaneous recovery of a source model in terms of its moment tensor components and the crustal structure along the propagation path between the source and the station (Mao *et al.* 1994; Chen *et al.* 2000).

Stations PDH and MBA are located within a sedimentary area (Fig. 1), so data from station ITK were used for modelling of a single station (Fig. 2). To obtain the best fit, the event depth had to be varied. Fig. 4(a) shows the best fit achieved between observed and synthetic data. In general, there is a good fit between observed and synthetic data when compared with the fit for the same station based on the initial K-model exhibited in Fig. 3. A phase shift can be seen on a free surface converted S to P phase, *SP*, and to a lesser degree, also on the S phase. To correct for this, the structure was perturbed by changing the value of Vp/Vs used to 1.72 and again allowing

© Royal Astronomical Society • Provided by the NASA Astrophysics Data System

2002GeoJI.151..221F

Table 8. Moment tensor inversion results and fault plane solutions of the selected events obtained by using F-model and a single station, that is, station ITK above (a), and partial multistation below (b).

	1	2	3
(a)			
M_{xx} ($\times 10^{12}$ N m)	0.893 ± 0.084	1.690 ± 0.087	0.438 ± 0.039
M_{yy} ($\times 10^{12}$ N m)	1.130 ± 0.059	-0.469 ± 0.040	0.072 ± 0.012
M_{xy} ($\times 10^{12}$ N m)	-1.530 ± 0.115	0.795 ± 0.079	-0.113 ± 0.009
M_{xz} ($\times 10^{12}$ N m)	1.460 ± 0.067	-6.920 ± 0.472	0.926 ± 0.033
M_{yz} ($\times 10^{12}$ N m)	-1.240 ± 0.049	0.997 ± 0.076	-0.201 ± 0.008
M_0 ($\times 10^{12}$ N m)	2.230	6.810	1.000
M_w	2.7	3.3	2.0
$E_{\rm rms}$ (μm)	0.38	0.24	0.12
Strike (deg)	36, 228	320, 82	72, 257
Dip (deg)	25, 65	10, 85	14, 76
Slip (deg)	-101, 85	-33, 98	-95, -89
Depth (km)	17.4	18.1	15.5
CLVD per cent	32	6	6
	Trend Plunge	Trend Plunge	Trend Plunge
P axis	149 69	344 52	172 57
T axis	315 17	178 40	344 29
(b)			
M_{xx} ($\times 10^{12}$ N m)	0.868 ± 0.119	1.480 ± 0.116	0.373 ± 0.058
M_{yy} ($\times 10^{12}$ N m)	0.898 ± 0.084	-0.376 ± 0.051	0.114 ± 0.017
M_{xy} ($\times 10^{12}$ N m)	-1.340 ± 0.167	0.662 ± 0.021	-0.104 ± 0.014
M_{xz} ($\times 10^{12}$ N m)	0.679 ± 0.067	-5.910 ± 0.222	1.040 ± 0.045
M_{yz} ($\times 10^{12}$ N m)	-0.612 ± 0.039	-0.819 ± 0.465	-0.228 ± 0.011
$E_{\rm rms}$ (μm)	0.81	0.367	0.17
Strike (deg)	42, 226	318, 83	67, 257
Dip (deg)	33, 57	10, 84	11, 79
Slip (deg)	-93, -88	-35, -98	-99, -88
Depth (km)	17.4	18.1	15.5
CLVD per cent	38	6	8
	Trend Plunge	Trend Plunge	Trend Plunge
P axis	143 80	344 52	172 57
T axis	315 11	178 40	344 34

the hypocenter position to change by varying the focal depth of the event. This resulted in a better fit for all phases, that is, *P*, *SP* and *S*, on all three components (Fig. 4b). Results in Table 4 show a significant improvement in the value of $E_{\rm rms}$ and estimated standard error for the components of moment tensor. On average, the standard errors are less than 10 per cent of the values of components. The decrease in the value of CLVD is an indication of an improved structural model along the propagation path. The increase in scalar seismic moment can be explained by the better fit especially to energetic phases, that is, *S* and *SP*, in all components. The fault plane solution, on the other hand, shows relatively small changes. This indicates that the improved solution obtained by a better fit of *SP* phase constrained the existing moment tensor solution by improving the standard errors.

From the hypocenter solution in Table 5, it can be seen that take-off angles for all fitted phases in Fig. 4(b) are greater than 90°. This implies that the improved fit only improves the propagation structure above the focal depth, that is, above 18.1 km. To improve the structure below the focal depth, information from down going phases and strong multiple reflected phases is required. This information can be obtained by fitting strong multiply reflected phases which are normally observed after the direct *P* and *S* phase (Arvidsson & Kulhanek 1994). To include such phases, the time window was increased from 9.0 s to 12.5 s. Again, the best fit was achieved by perturbing the phase velocity and the thickness of the third layer, and the position of the Moho depth, while fixing the focal depth of the event at 18.1 km to the improved K-model. Fig. 4(c) compares the fit from the two structures. As expected, the fit to the data obtained from the two structures is similar up to the end of the direct *S* phase. From then a modified structure (subsequently referred to as the F-model) shows a relatively good fit especially on the transverse component although the radial component is not well fitted. The improvement is also reflected in values of $E_{\rm rms}$ obtained for the two cases (Table 6). Again, fault plane solutions based on the two structures show only small differences.

Finally, for the sake of comparison between different structures, we also generate synthetic seismograms based on the structure of Camelbeeck & Iranga (1996) (subsequently referred to as the C & I-model). Results from this model were compared with the other two models, that is, with the K-model and the F-model. Fig. 5 shows the fit from the three models and Table 7 summarizes the results. The value of $E_{\rm rms}$ obtained by using the F-model is comparatively small. The large estimated value of the scalar seismic moment obtained using the C & I-model can be explained by the location of station ITK close to a nodal plane (Tables 5 and 7). Hence, a small change in the estimated location associated with the change in structure can lead to a large change in seismic moment without significant change in the fault orientation (Koch 1991b).

Once we had obtained a good fit between the observed and synthetic data and a small error in the moment tensor components, we decided to use the F-model to calculate the Green's functions of the other two events recorded at station ITK (Table 2). Final results for all three events are listed in Table 8(a). Fig. 6 shows the fit

© Royal Astronomical Society • Provided by the NASA Astrophysics Data System

2002GeoJI.151..221F

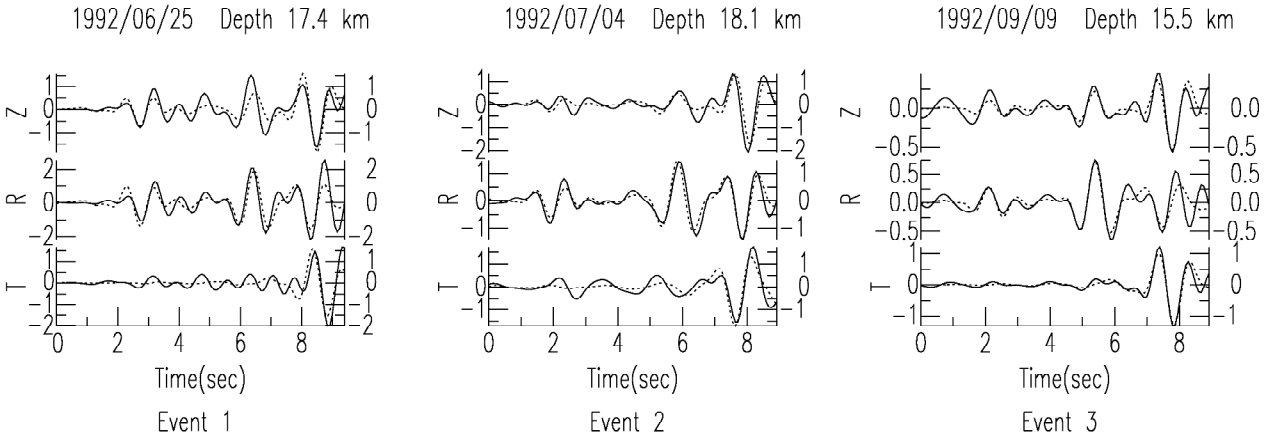


Figure 6. Single station moment tensor results of the selected events based on synthetics generated using the F-model.

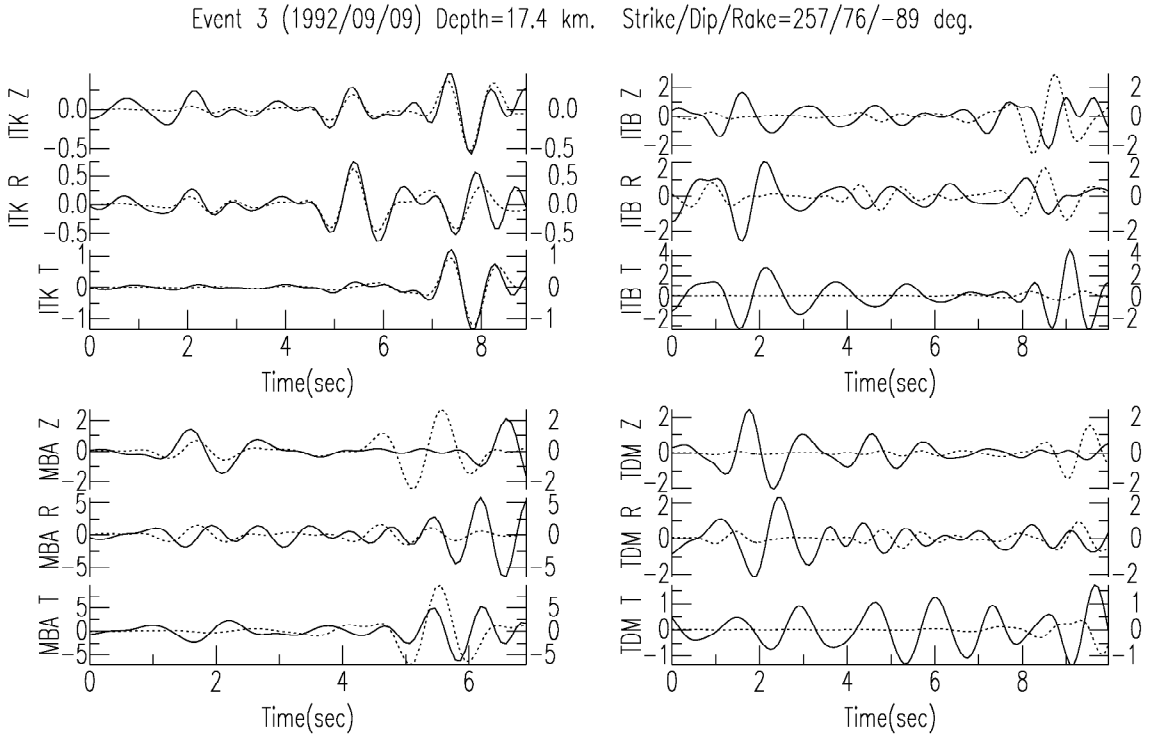


Figure 7. The forward modelling results obtained when the best single-station double-couple solution of event 3, based on station ITK, is applied to the other stations where the event is recorded.

between the observed records and synthetics for all of the events. In all cases the prominent phases have been predicted well. Despite being small in magnitude, event 3 shows a comparatively better fit (Table 8a). From Fig. 6 it is seen that all solutions support a dip slip mechanism. Event 1 is orientated NE–SW, while the other two are orientated ENE–WSW. Moment magnitudes obtained show that event 2 is larger than event 1 in contradiction to the results of Camelbeeck & Iranga (1996).

4.2 Multistation solution

Although theoretically a single station moment tensor solution is acceptable (Stump & Johnson 1977; Langston 1979), in practice there are cases where the solution is not unique (Singh *et al.* 2000). Therefore we tried to find ways to constrain our single station solutions obtained as in the preceding section by adding data from other stations. This was done through forward modelling based on single station results for all stations where the events were recorded, to see how predicted seismograms deviated from those observed. Fig. 7 shows a multistation fit of event 3 based on the ITK single station solution. It can be seen that a fit has not been achieved for the further stations, that is, ITB and TDM. This is because the band-pass filter chosen was unable to resolve prominent phases for such a low-magnitude event at an epicentral distance of 70 km. Examining the fit at two near stations, that is, ITK and MBA in Fig. 7, one can see a phase shift for the *P* phase on both vertical and radial

© Royal Astronomical Society • Provided by the NASA Astrophysics Data System

2002GeoJI.151..221F

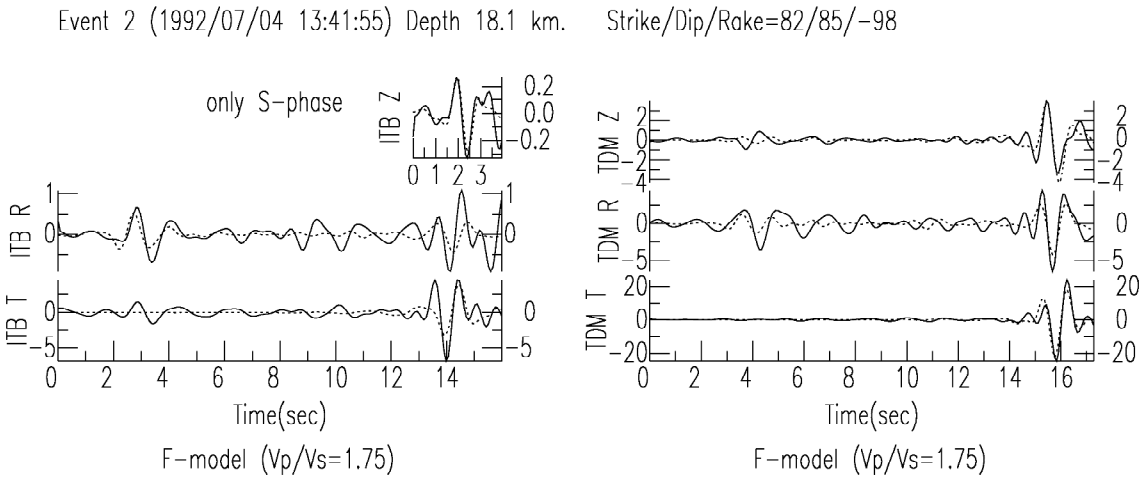


Figure 8. The forward modelling results obtained after propagation correction, when the best single-station double-couple solution of event 2 based on station ITK is applied to station ITB and TDM.

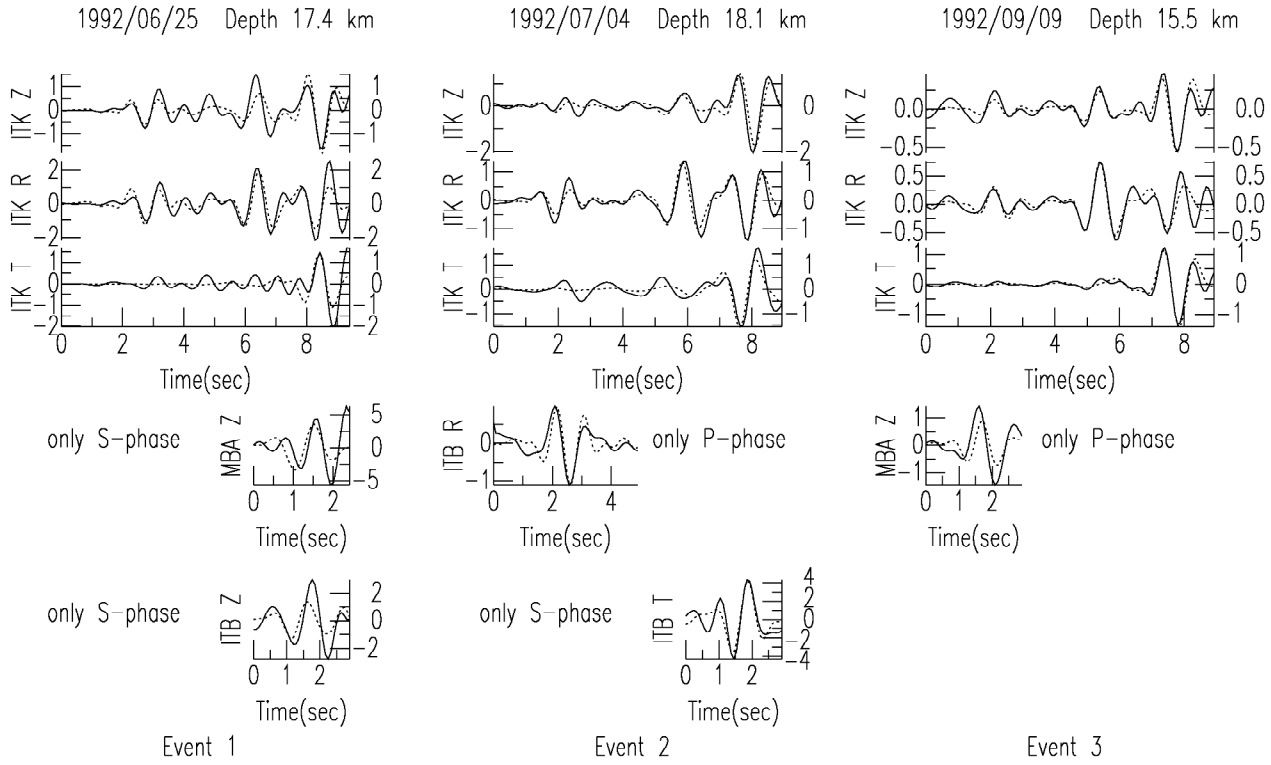


Figure 9. Partial multistation moment tensor inversion results for the three selected events.

components and for the *S* on the transverse component at station MBA. For this station, there is also an amplitude mismatch on both *P* and *S* phases. When traces on the vertical and transverse components are compared a clear delay of an observed *S* phase on a vertical component is visible. We will try to address these observations in order to explain why the data from station MBA are not consistent with the single station solution used.

The observed time shifts and amplitude mismatch within the given frequency band are associated with location inaccuracy and structural heterogeneity along the propagation paths to the two stations. Since the program we used for computing the Green's functions uses a homogeneous horizontally layered model, making use of the best solution based on the propagation path to station ITK leads to a poor phase fit for the path to station MBA path as the structure along the propagation paths is significantly different (Fig. 1). A question which naturally follows from this is whether or not the use of 1-D model in the inversion procedure is adequate? To investigate this, we took the source parameters estimated using a single station analysis, and then used these parameters to simulate (forward model) the signal expected at the other stations, but now using the

© Royal Astronomical Society • Provided by the NASA Astrophysics Data System

2002GeoJI.151..221F

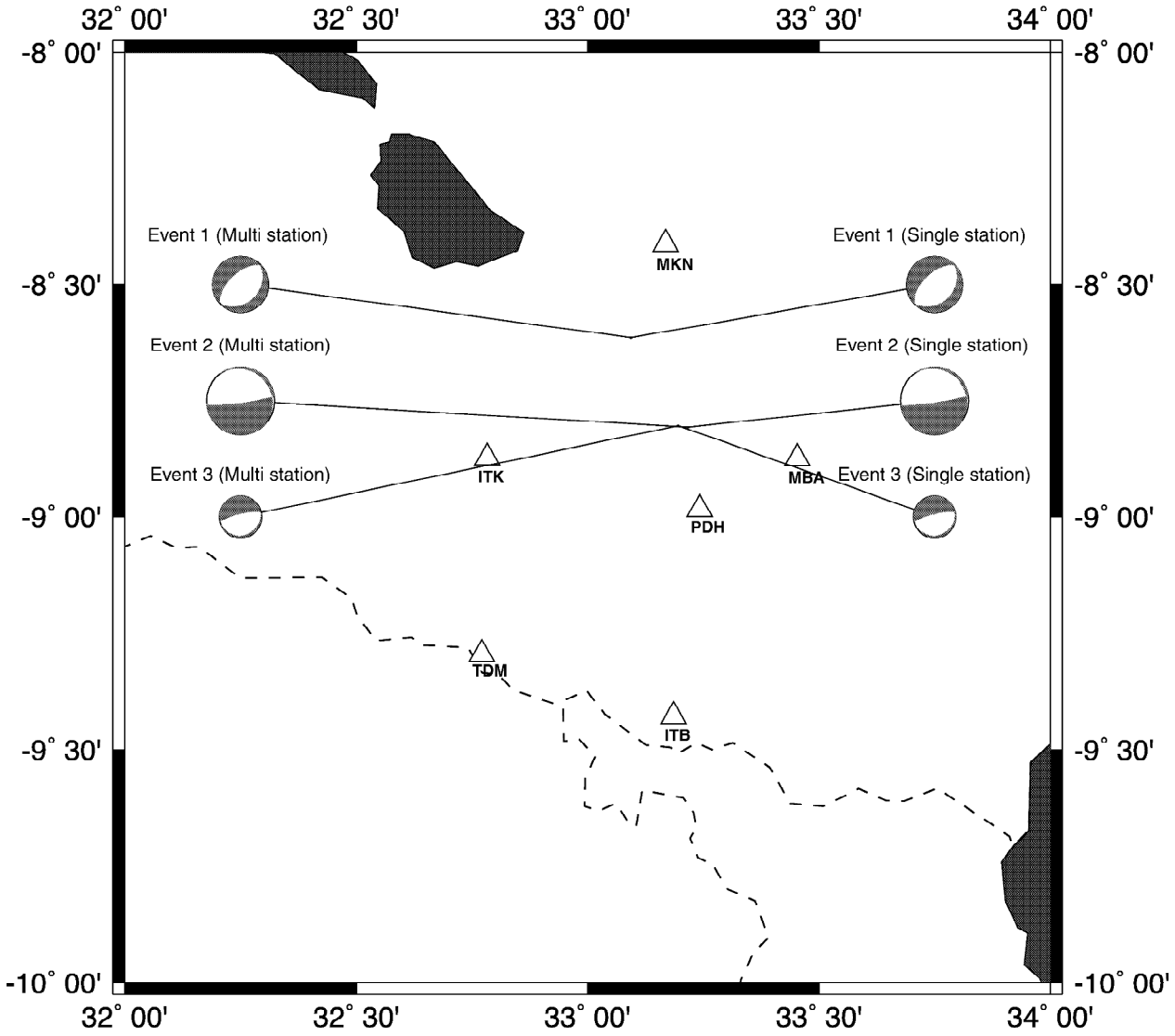


Figure 10. Comparison between fault plane solutions determined by using a single station and multistation for the three selected events along the Rukwa rift.

best 1-D structure for each of these stations, as estimated beforehand using a single station analysis for each of respective station. Some results are illustrated in Fig. 8. It can be seen that, while not perfect, the fit between the real and simulated data is reasonable, implying that our 1-D approximation is adequate in this type of analysis.

For our experimental configuration, frequency band and plausible values of the possible errors in the estimated source location, these errors may have a significant effect on the travel times to the stations. Furthermore, the amplitudes observed at a given station may be perturbed due to differences in the radiation pattern between the true and estimated source locations. The source depth may also strongly affect the waveform due to interference effects between the direct and surface reflected parts of the observed signals. Apart from the effect of the radiation pattern, site effects, especially in sedimentary areas, are also contributing factors. Some workers, for instance Zhu & Helmberger (1996) and Chen *et al.* (2000), invoke the concept of site corrections to explain some of the amplitude discrepancies between observed and synthetic data. As some of our data is recorded in areas with significant sedimentary cover and some in areas without, the effects local to the stations could also be expected to be significant for some of our data.

The third observation, that is, delay of observed direct *S* phase on the vertical component, may be explained by destructive interference between the *S* and *SP* phases. Although at station ITK, 46 km from the source, the maximum amplitudes of the two phases seemed unequal (Fig. 7), at station MBA (30 km) the two phases may be expected to have very similar amplitudes as the *SP* phase is just around the critical distance, where their sizes are comparable but of opposite polarity.

With the explanations above, we decided to incorporate only phases for which the observed time-shift between observed and synthetic data was minimal. This was done by taking a short window around the phase, that is, *P* or *S* and using its onset time rather than the origin time for alignment (Schurr & Nabelek 1999). In the present work, no attempt at amplitude correction using a site effect

© Royal Astronomical Society • Provided by the NASA Astrophysics Data System

2002GeoJI.151..221F

concept was applied. Table 8(b) summarizes the partial multistation results for the three events. The slight increase in values of E_{rms} and CLVD as compared with results from a corresponding single station analysis reflects the propagation and site effects which could not be accounted for because of the use of an inappropriate structural model (Sileny *et al.* 1992). From Fig. 9 it can be seen that all three events still support a dip slip mechanism.

Fig. 10 shows a comparison of the 'beach balls' obtained using the single station and partial multistation solutions. From the figure, 'beach balls' for all three events look similar. From Table 8, it can be seen that the CLVD percentage of event 1 is comparatively high (above 30 per cent). It is also larger than the average error value observed on components of moment tensor for all three events, that is, 10 per cent. Systematic studies on Harvard centroid moment tensor solutions with significant non-double couple components (NDCC) have shown that the NDCC is a result of both inadequacies in the structure model and source complexity (Kuge & Lay 1994a,b; Frohlich 1995). Frohlich (1994), describe the complexity as due to an earthquake with two or more subevents, separated in space and in time, occurring on suitably oriented non-parallel faults. Since, in this study, the minimum fit between the data and synthetics was achieved by perturbing the structural model, we suspected that the large CLVD percentage for event 1 may be associated with the source complexity. The event location and the orientation of the DC component lie in an accommodation zone marked by a buried ridge that links the Lupa and Songwe border faults along the Rukwa rift (Peirce & Lipkov 1988; Ebinger *et al.* 1989). However, with only one event analysed in this area, it is less a statistically meaningful conclusion than an indication of need for further work.

5 CONCLUSIONS

In this paper we have demonstrated the power of the moment tensor inversion technique to retrieve the source parameters of small earthquakes. We have also shown that, at short epicentral distances a better fit to observed free surface converted phases such as *SP* and multiply reflected phases arriving after the direct *S* phase can contribute to improving estimates of the focal parameters, event location (especially depth) and the structure along the propagation path.

At least for the data analysed in this study, it appears that analysis using a 1-D earth model can provide reliable results, but that different 1-D models are necessary for different propagation paths.

ACKNOWLEDGMENTS

RWF acknowledges financial support from the International Science Program (IPPS section) and the Department of Earth Sciences of Uppsala University and would like to express special thanks to L. Hasselgren, Director of IPPS, for initiating the Tanzanian seismic project. RA was partially supported by the Swedish International Agency's developing countries' research council (SAREC; contract SWE-1997-319 and contract SWE-2000-323). We appreciate the comments given by O. Kulhanek, R. Roberts and R. Slunga and other anonymous reviewers after critically reading the manuscript. We express our gratitude to the Seismology group at the Royal Observatory of Belgium and the of the University of Dar es Salaam, Tanzania for providing us with the data from the Mbeya network. This work was carried out at the Department of Earth Sciences, Seismology Programme, Uppsala University.

REFERENCES

Aki, K. & Richards, P.G., 1980. *Quantitative Seismology: Theory and Methods*, Vol. I, W.H. Freeman, San Francisco.

Arvidsson, R., 1996. Fennoscandian earthquakes: Whole crustal rupturing related to postglacial rebound, *Science,* **274,** 744–746.

Arvidsson, R. & Kulhanek, O., 1994. Seismodynamics of Sweden deduced from earthquake focal mechanisms, *Geophys. J. Int.,* **116**, 377–392.

Bouchon, M., 1981. A simple method to calculate Green's functions for elastic layered media, *Bull. seism. Soc. Am.,* **71**, 959–971.

Camelbeeck, T. & Iranga, M.D., 1996. Deep crustal earthquakes and active faults along the Rukwa trough, eastern Africa, *Geophys. J. Int.,* **124**, 612–630.

Chen, J., Helmberger, D.V. & Wald, D.J., 2000. Basin structure estimation by waveform modeling: forward and inverse methods, *Bull. seism. Soc. Am.,* **90**, 964–976.

Dziewonski, A. & Woodhouse, J., 1983. An experiment in the systematic study of global seismicity: Centroid moment tensor solutions for 201 moderate and large earthquakes of 1981, *J. geophys. Res.,* **88**, 3247 3271.

Ebinger, C.J., Deino, A.L., Drake, R.E. & Tesha, A.L., 1989. Chronology of volcanism and rift basin propagation: Rungwe volcanic province, East Africa, *J. geophys. Res.,* **94**, 15 785–15 803.

Fan, G. & Wallace, T., 1991. The determination of source parameters for small earthquakes from a single, very broadband seismic station, *Geophys. Res. Lett.,* **18**, 1385–1388.

Ferdinand, R.W., 1998. Average attenuation of 0.7–5.0 Hz Lg waves and magnitude scale determination for the region bounding the western branch of the East African rift, *Geophys. J. Int.,* **134**, 818–830.

Ferdinand, R.W. & Camelbeeck, T., 2000. Regional phases from earthquakes along the western branch of the East African rift and relocation of epicenters between 1°N and 12°S., *African Geoscience Review,* **7**, 273–287.

Frohlich, C., 1994. Earthquakes with non-double-couple mechanisms, *Science,* **264**, 804–809.

Frohlich, C., 1995. Characteristics of well-determined non-double-couple earthquakes in the Harvard CMT catalog, *Phys. Earth planet. Inter.,* **91**, 213–228.

Geller, R.J., 1976. Body force equivalents for stress-drop seismic sources, *Bull. seism. Soc. Am.,* **66**, 1801–1804.

Gilbert, F., 1970. Excitation of the normal modes of the Earth by earthquake sources, *Geophys. J. R. astr. Soc.,* **22**, 223–226.

Given, J., Wallace, T. & Kanamori, H., 1982. Teleseismic analysis of the 1980 Mammoth Lakes earthquake sequence, *Bull. seism. Soc. Am.,* **72**, 1093–1109.

Hanks, T.C. & Kanamori, H., 1979. A moment magnitude scale, *J. geophys. Res.,* **84**, 2348–2350.

Havskov, J., 1997. *The SEISAN Earthquake Analysis Software for IBM PC and SUN,* Version 6.0, Institute of Solid Earth Physics, University of Bergen.

Helmberger, D.V. & Johnson, L.R., 1977. Source parameters of moderate size earthquakes and the importance of receiver crustal structure in interpreting observations of local earthquakes, *Bull. seism. Soc. Am.,* **67**, 301–313.

Herrmann, R.B., 1996. *Computer Programs in Seismology,* Version 3.0, Department of Earth and Atmospheric Sciences, Saint Louis University.

Herrmann, R.B. & Wang, C.Y., 1985. A comparison of synthetic seismograms, *Bull. seism. Soc. Am.,* **74**, 41–56.

Jost, M.L. & Herrmann, R.B., 1989. A student's guide and review of moment tensors, *Seism. Res. Lett.,* **60**, 37–57.

Kim, W.-Y., 1987. Modelling short-period crustal phases at regional distances for the seismic source parameter inversion, *Phys. Earth planet. Inter.,* **47**, 159–177.

Klein, F.W., 1984. Users guide to HYPOINVERSE, a program for Vax and PC350 computers to solve for earthquake locations, *USGS open file report,* 84-000.

Koch, K., 1991a. Moment tensor inversion of local earthquake data—I. Investigation of the method and its numerical stability with model calculations, *Geophys. J. Int.,* **106**, 305–319.

© Royal Astronomical Society • Provided by the NASA Astrophysics Data System

2002GeoJI.151..221F

Koch, K., 1991b. Moment tensor inversion of local earthquake data—II. Application of aftershocks of the May 1980 Mammoth Lakes earthquakes, *Geophys. J. Int.,* **106**, 321–332.

KRISP Working Party, 1991. Large-scale variation in lithospheric structure along and across Kenya rift, *Nature,* **354**, 223–227.

Kuge, K. & Lay, T., 1994a. Data-dependent non-double-couple components of shallow earthquake source mechanisms: Effects of waveform inversion instability, *Geophys. Res. Lett.,* **21**, 9–12.

Kuge, K. & Lay, T., 1994b. Systematic non-double-couple components earthquake mechanisms: The role of fault zone irregularity, *J. geophys. Res.,* **99**, 15 457–15 467.

Langston, C.A., 1979. A single-station fault-plane solution method, *Geophys. Res. Lett.,* **6**, 41–44.

Langston, C.A. & Helmberger, D.V., 1975. A procedure for modelling shallow dislocation sources, *Geophys. J. R. astr. Soc.,* **42**, 117–130.

Lay, T. & Wallace, T., 1995. *Modern Global Seismology, International Geophysics Series 58,* Academic Press, San Diego.

Maguire, P.K.H. & Long, R.E., 1976. The structure on the western flank of the Gregory rift (Kenya). Part I. The crust, *Geophys. J. R. astr. Soc.,* **44**, 661–675.

Mao, W.J., Panza, G.F. & Sulhadolc, P., 1994. Linearized waveform inversion of local and near-regional events for source mechanism and rupturing processes, *Geophys. J. Int.,* **116**, 784–798.

Nabelek, J.L., 1984. Determination of earthquake source parameters from inversion of body waves, *PhD thesis,* Massachusetts Institute of Technology, Cambridge.

Nabelek, J. & Xia, G., 1995. Moment-tensor analysis using regional data: application to the 25 March, 1993, Scotts Mills, Oregon, earthquake, *J. geophys. Res.,* **22**, 13–16.

Nolet, G. & Muller, S., 1982. A model for the deep structure of the East African rift system from simultaneous inversion of teleseismic data, *Tectonophysics,* **84**, 151–178.

Peirce, J.W. & Lipkov, L., 1988. Structural interpretation of the Rukwa rift, Tanzania, *Geophysics,* **53**, 824–836.

Saikia, C.K. & Herrmann, R.B., 1985. Application of waveform modeling to determine focal mechanisms of four 1982 Miramichi aftershocks, *Bull. seism. Soc. Am.,* **75**, 1021–1040.

Schurr, B. & Nabelek, J.L., 1999. New techniques for the analysis of earthquake sources from local array data with an application to the 1993 Scotts Mills, Oregon, aftershock sequence, *Geophys. J. Int.,* **137**, 585–600.

Shomali, Z.H. & Slunga, R., 2000. Body wave moment tensor inversion of local earthquakes: an application to the South Iceland seismic zone, *Geophys. J. Int.,* **140**, 63–70.

Sileny, J. & Pšenčik, I., 1995. Mechanisms of local earthquakes in 3-D inhomogeneous media determined by waveform inversion, *Geophys. J. Int.,* **121**, 459–474.

Sileny, J., Panza, G.F. & Campus, P., 1992. Waveform inversion for point source moment tensor retrieval with variable hypocentral depth and structural model, *Geophys. J. Int.,* **109**, 259–274.

Sileny, J., Campus, P. & Panza, G.F., 1996. Seismic moment tensor resolution by waveform inversion of a few local noisy records—I. Synthetic tests, *Geophys. J. Int.,* **126**, 605–619.

Singh, S.K., Ordaz, M., Pacheco, J.F. & Courboulex, F., 2000. A simple source inversion scheme for displacement seismograms recorded at short distances, *J. Seism.,* **4**, 267–284.

Sipkin, S.A., 1986. Estimation of earthquake source parameters by the inversion of waveform data, global seismicity 1981–1983, *Bull. seism. Soc. Am.,* **76**, 1515–1541.

Stump, B.W. & Johnson, L.R., 1977. The determination of source properties by the linear inversion of seismograms, *Bull. seism. Soc. Am.,* **67**, 1489–1501.

Zhao, L-S. & Helmberger, D.V., 1994. Source estimation from broadband regional seismograms, *Bull. seism. Soc. Am.,* **84**, 91–104.

Zhao, M., Langston, C.A., Nyblade, A.A. & Owens, T.J., 1997. Lower crustal rifting in the Rukwa graben, East Africa, *Geophys. J. Int.,* **129**, 412–420.

Zhu, L. & Helmberger, D.V., 1996. Advancement in source estimation techniques using broadband regional seismograms, *Bull. seism. Soc. Am.,* **86**, 1634–1641.

© Royal Astronomical Society • Provided by the NASA Astrophysics Data System